

Supporting Information for

Crystal Structure Design and Multiband Physical Properties of Quaternary Sulfide $\text{Ba}_5\text{Bi}_2\text{Co}_2\text{S}_{10}$ for Optoelectronic Conversion

Kejun Bu,^{†, ‡} Xian Zhang,^{*, ‡} Jian Huang,[†] Mengjia Luo,^{†, ‡} Chong Zheng,[#] Ruiqi Wang,[§]
Dong Wang,^{†, ‡} Jianqiao He,^{†, ‡} Wei Zhao,[†] Xiangli Che,^{*, †} and Fuqiang Huang^{*, †, §}

[†]State Key Laboratory of High Performance Ceramics and Superfine Microstructure, Shanghai Institute of Ceramics, Chinese Academy of Sciences, Shanghai 200050, P. R. China

[‡]University of Chinese Academy of Sciences, Beijing 100049, China

[‡]Qian Xuesen Laboratory of Space Technology, China Academy of Space Technology, Beijing 100094, P. R. China

[§]State Key Laboratory of Rare Earth Materials Chemistry and Applications, College of Chemistry and Molecular Engineering, Peking University, Beijing 100871, P.R. China

[#]Department of Chemistry and Biochemistry, Northern Illinois University, DeKalb, Illinois 60115, United States

List of contents:

- 1. Experimental section.**
- 2. Supplementary Figures.**
- 3. Supplementary Tables.**

1. Experimental section.

Reagents. All starting materials were obtained from Alfa Aesar Puratronic, and used without further purification: (i) BaS powder, AR, 99%; (ii) bismuth powder, AR, 99.9%; (iii) cobalt powder, AR, 99%; (iv) sulfur powder, sublimed, 99.9%.

Synthesis of Ba₅Bi₂Co₂S₁₀ Single Crystals. All operations were carried out in Ar-protected glove box. Single crystal samples were synthesized by traditional melting salt method. A mixture of starting materials of BaS powder (2.5 mmol), Bi powder (1 mmol), Co powder (1 mmol), S powder (2.5 mmol), and KI powder (25 mmol) was loaded in a carbon-coated fused silica tube. The tube was evacuated to 10⁻³ mbar, sealed and heated gradually (60 Kh⁻¹) to 1273 K, where it was kept for two days. The tube was cooled to 773 K at a rate of 3 Kh⁻¹ and then quenched to room temperature. The direct combination reaction at the presence of excess KI flux gave solidified melts. The melts were washed and sonicated by distilled water and dried with alcohol. Then the black Ba₅Bi₂Co₂S₁₀ single crystals were obtained. The presence of Ba, Bi, Co, and S was confirmed by semi-quantitative energy-dispersive X-ray (EDX) analysis on a JEOL (JSM6510) scanning electron microscope (Figure S1). A number of different crystals were chosen, and their average Ba/Bi/Co/S atomic ratio was 25.71/11.77/9.10/53.42.

Single Crystal X-ray Crystallography. Suitable crystals were chosen to perform the data collections. Single crystal X-ray diffraction was performed on a Bruker D8QUEST diffractometer equipped with Mo *K* α radiation. The diffraction data were collected at room temperature by the ω - and φ - scan methods. The crystal structures were solved and refined using APEX3 program.¹ Absorption corrections were performed using the multi-scan method (ASDABS). The detailed crystal data and structure refinement parameters are

summarized in Table S2. Fractional atomic coordinates parameters, atomic displacement parameters and geometric parameters are summarized in Table S3-S5.

Powder X-ray Diffraction. The as-synthesized crystal samples were ground into fine powder before use. Phase purity of the powder samples was checked by powder X-ray diffraction performed on a Bruker D8QUEST diffractometer equipped with mirror-monochromatized source of Cu $K\alpha$ radiation ($\lambda = 0.15406$ nm). The patterns were recorded in a slow-scanning mode with 2θ from 5° to 80° at a scan rate of $2^\circ/\text{min}$. Simulated patterns were generated by using the CrystalMaker program and CIF file of the refined structure.

Physical Properties Measurements. Magnetic properties were measured on a Physical Properties Measurement System (PPMS, Quantum Design). Temperature-dependent direct-current (DC) magnetic susceptibility (M-T) curve of the powder sample was measured from 2 to 300 K under the magnetic field of 1 T in the zero field cooling (ZFC) and field cooling (FC) processes. The field dependence of magnetization was measured at 2 K, 10 K, 50 K, and 300 K under the applied magnetic field from -2 T to 2 T. Low-temperature electrical resistivity (2–300 K) and room-temperature Hall effect measurements (-2 T–2 T) were also measured using a PPMS. The formula $p = 1/R_H e$, was used to calculate the carrier concentration by the approximation of single parabolic band conduction model. The variable range hopping (VRH) model is a well-known model that can be used to describe the semiconducting transport. The VRH model can be expressed as:

$$\rho_T = \rho_0 \exp\left[\left(\frac{T_0}{T}\right)^{1/4}\right] \quad (1)$$

Where $T_0 = \frac{\beta}{\kappa g(\mu) a^3}$, $g(\mu)$ is the density of states at the Fermi level, a is the localization radius of the states near the Fermi level, and β is a numerical coefficient.

Solid-state UV/Vis and UPS spectroscopy. The solid-state ultraviolet-visible (UV-vis) light diffuse-reflectance spectra of the fine powders of $\text{Ba}_5\text{Bi}_2\text{Co}_2\text{S}_{10}$ were measured on a UV-4100 spectrophotometer operating from 1200 to 350 nm at room temperature. BaSO_4 powder was used as a 100% reflectance standard. The powder sample was spread on a compacted base of BaSO_4 powder. The generated reflectance-versus-wavelength data were used to measure the band gap of the as-synthesized samples. The reflectance data were converted to absorbance data by using the Kubelka-Munk equation.² The valence band level of the $\text{Ba}_5\text{Bi}_2\text{Co}_2\text{S}_{10}$ was determined by ultraviolet photoemission spectroscopy in Kratos Axis Ultra DLD multitechnique surface analysis system using He (21.21 eV) photon lines from a discharge lamp with an error about 0.01 eV.

Thermal Analyses. Thermogravimetric analysis (TG) and Differential Scanning Calorimeter (DSC) carried out on a NETZSCH STA449C thermal analyzer for investigating the thermal properties of the $\text{Ba}_5\text{Bi}_2\text{Co}_2\text{S}_{10}$ compound. A well-ground powder sample (10.51 mg) was loaded into an Al_2O_3 crucible and heated from room temperature to 1000 °C at 10 °C/min under a constant flow of argon gas.

Photoelectric properties. The ceramic sample was prepared by pressing the sample powder into a pellet with a diameter of 8 mm under a pressure of 15 Mpa. Then the pellet was sealed in an evacuated quartz tube and sintered into a compacted ceramic pellet under 723 K for 5 h. Photocurrent density-voltage (J - V) characteristics were measured under visible light with a 300 W xenon lamp (filter: $\lambda = 420$ nm), which is a standard solar light

intensity. The light intensity was calibrated with an NREL-calibrated Si cell (Oriel 91150). Current-voltage (I - V) measurements were performed by sweeping the voltage from the positive maximum to the negative minimum using a semiconductor characterization system (KEITHLEY 4200).

Electronic Structure Calculation. Density functional theory (DFT) calculations were performed using the Vienna Ab Initio Simulation Package (VASP).³⁻⁵ The Perdew-Burke-Ernzerhof (PBE) version of the generalized gradient approximation (GGA) was used to describe the exchange correlation functional, and the projector augmented wave (PAW) method was used in the present work.⁶ Here the cutoff energy of plane wave was chosen at 400 eV. For the structure optimizations, $8 \times 6 \times 8$ k-points were used for the conventional cell. The convergence criteria are that the changes in total energies between two successive electronic steps are less than 10^{-5} eV, and all the Hellmann-Feynman force acting on each atom is less than 0.01 eV /Å. High-symmetry points in Brillouin zones (B, Γ , C, Z, E and Y represent (0, 0, 0.5), (0, 0, 0), (0.5, 0.5, 0), (0, 0.5, 0), (-0.5, 0.5, 0.5) and (0.5, 0, 0)) were considered in our band structure calculation. The calculations about work function are also based on DFT calculations, as implemented in the VASP. The (hkl) surface is simulated using a slab model: slabs in the (hkl) crystallographic direction, are generated with at least eight atomic planes. A vacuum thickness of 12 Å is set between two periodically repeated slabs. Each slab is symmetrical to avoid unphysical dipole–dipole interactions between two consecutive slabs.

2. Supplementary figures.

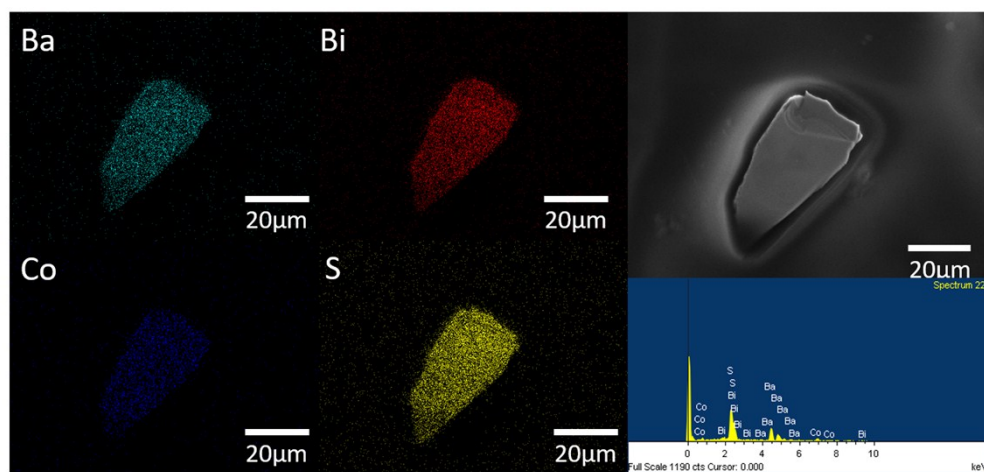


Figure S1. The SEM image and EDS result of $\text{Ba}_5\text{Bi}_2\text{Co}_2\text{S}_{10}$ crystal, and element mapping of Ba, Bi, Co and S in $\text{Ba}_5\text{Bi}_2\text{Co}_2\text{S}_{10}$.

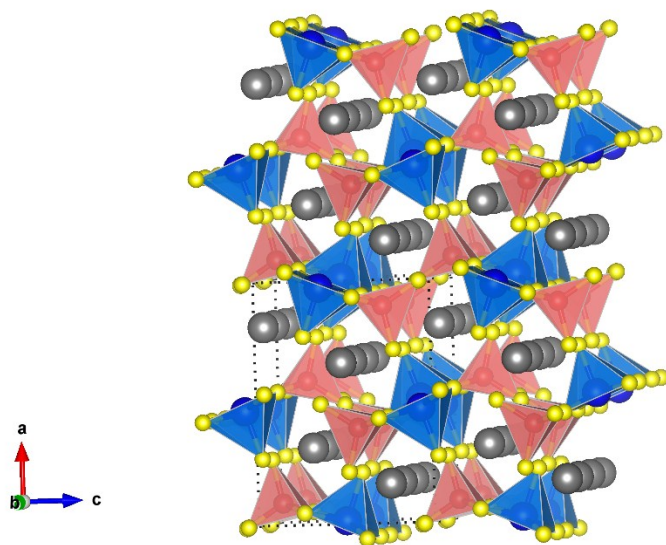


Figure S2. Crystal structure of $\text{Ba}_2\text{BiFeS}_5$ viewed down the b -axis.⁷

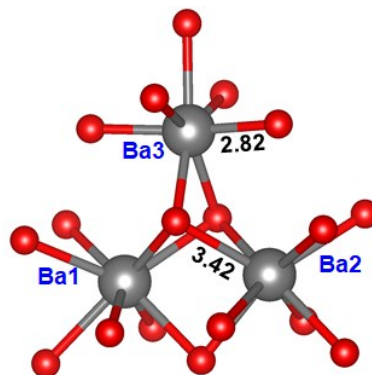


Figure S3. Coordination environment of Ba1, Ba2 and Ba3.

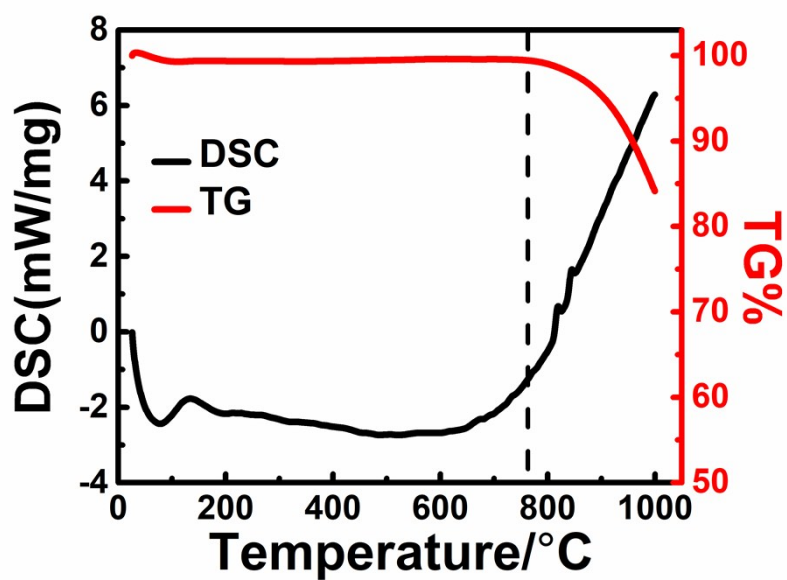


Figure S4. DSC (black) and TG (blue) diagrams of $\text{Ba}_5\text{Bi}_2\text{Co}_2\text{S}_{10}$.

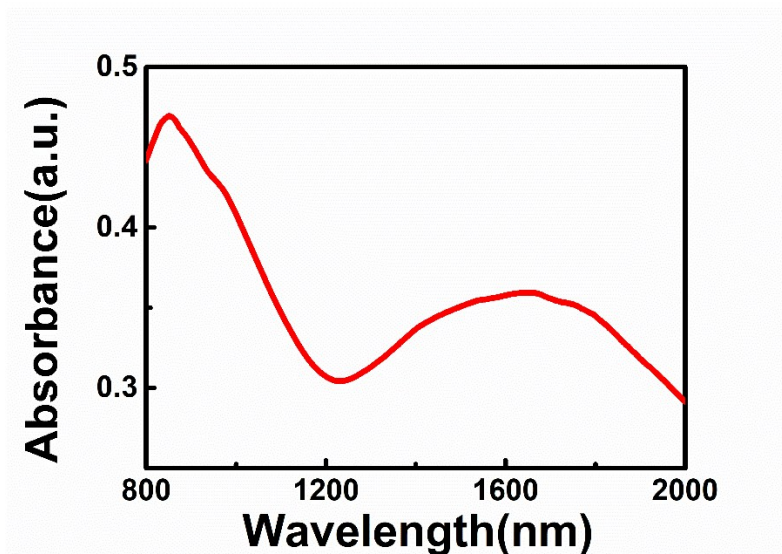


Figure S5. Solid-state UV-vis absorption spectra of Ba₅Bi₂Co₂S₁₀.

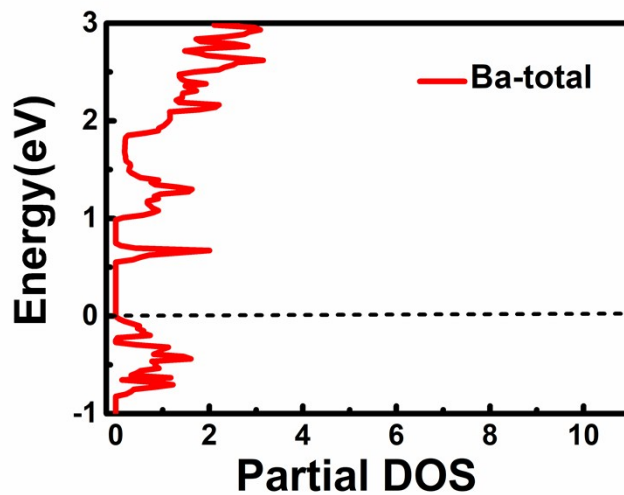


Figure S6. The total density of states of Ba²⁺ ions in Ba₅Bi₂Co₂S₁₀.

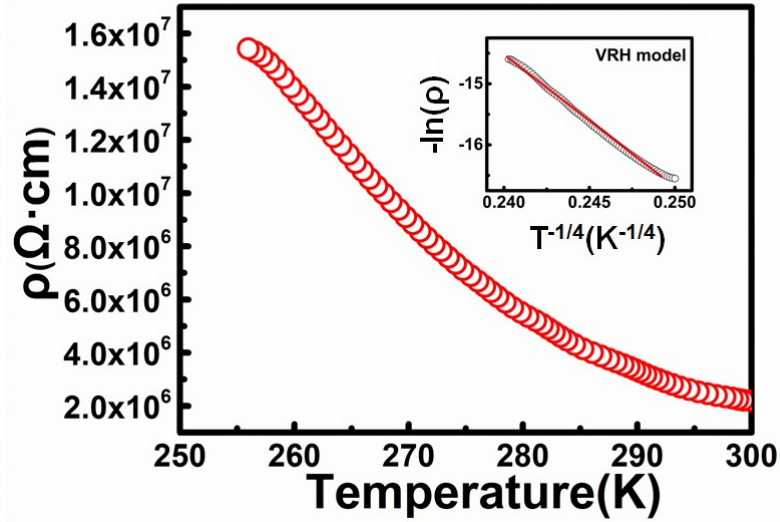


Figure S7. Resistivity versus temperature profile for $\text{Ba}_5\text{Bi}_2\text{Co}_2\text{S}_{10}$. Insets: Plots of $\ln \rho$ vs $T^{-1/4}$ (VRH model).

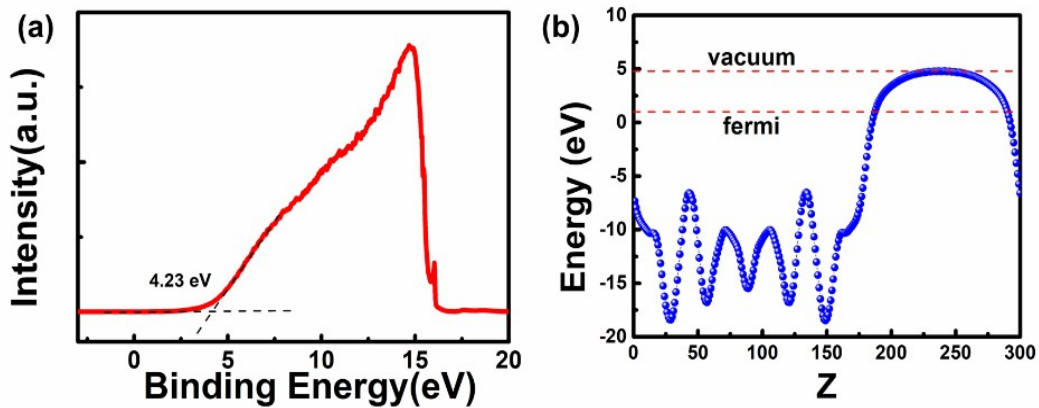


Figure S8. (a) The UPS spectrum of the $\text{Ba}_5\text{Bi}_2\text{Co}_2\text{S}_{10}$. (b) Theoretically calculated electronic properties of $\text{Ba}_5\text{Bi}_2\text{Co}_2\text{S}_{10}$: the work function.

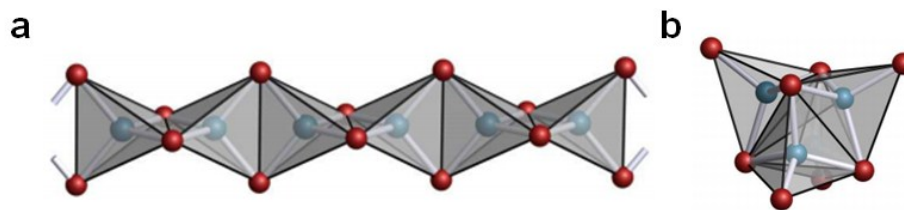


Figure S9. (a) ${}^1\infty[\text{CoO}_2]^{2-}$ 1D infinite chains and (b) $[\text{Co}_4\text{Se}_8]^{7-}$ anion clusters.⁸⁻⁹

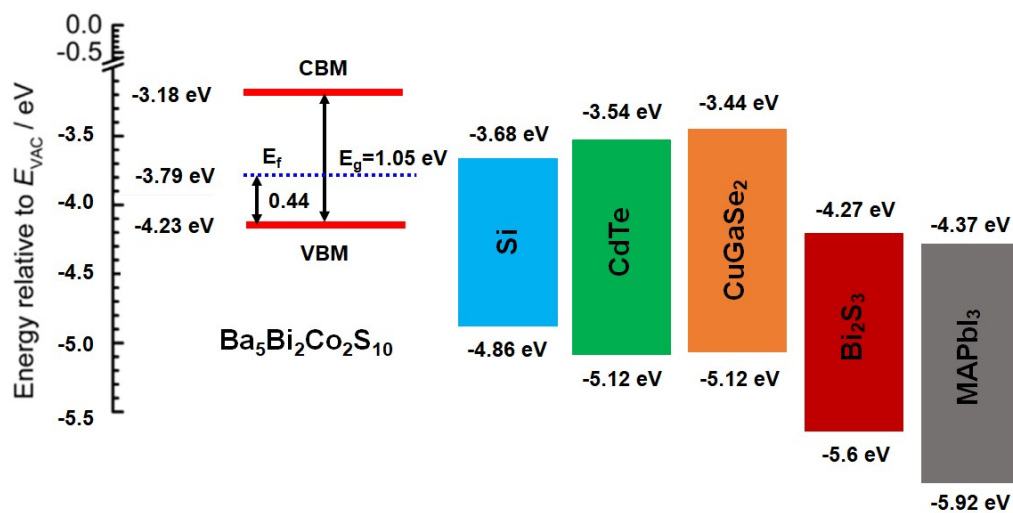


Figure S10. Schematic band position of $\text{Ba}_5\text{Bi}_2\text{Co}_2\text{S}_{10}$ with respect to the vacuum level (E_{VAC}), which is compared with some well-known semiconductors.¹⁰

3. Supplementary tables.

Table S1. EDS results of $\text{Ba}_5\text{Bi}_2\text{Co}_2\text{S}_{10}$.

Element	Weight%	Atomic%
S K	20.79	53.42
Co K	6.51	9.10
Ba L	42.86	25.71
Bi M	29.84	11.77
Totals	100.00	100.00

Table S2. Crystal Data and Details of the Structure Refinements for Ba₅Bi₂Co₂S₁₀.

Chemical formula	Ba ₅ Bi ₂ Co ₂ S ₁₀
F _w (g·mol ⁻¹)	1543.07
Crystal system	Monoclinic
Space group	P2 ₁ /m
<i>a</i> , (Å)	8.9913(5),
<i>b</i> , (Å)	12.5989(6),
<i>c</i> , (Å)	9.1253(5)
α (deg)	90
β (deg)	104.664(2)
γ (deg)	90
V (Å ³)	1000.05(9)
Temperature (K)	293
Z	2
Crystal color	Black
ρ_c (g·cm ⁻³)	5.125
μ (mm ⁻¹)	29.84
F(000)	1320
R _{int}	0.056
R ₁ [<i>I</i> > 2 σ (<i>I</i>)]	0.028
wR ₂ (all data)	0.051
GOF	1.03

$\alpha R_1 = \sum ||F_o| - |F_c|| / \sum F_o$. $wR_2 = [\sum w(F_o^2 - F_c^2)^2 / \sum w(F_o^2)^2]^{1/2}$.

REFERENCES

1. Sheldrick, G. *Acta Crystallogr., Sect C.* 2015, **71**, 3-8.
2. Kortüm, G.; Braun, W.; Herzog, G. *Angew. Chem. Int. Ed.* 1963, **2**, 333-341.

3. Kresse, G.; Hafner, J. *Phys. Rev. B.* 1993, **47**, 558-559.
4. Kresse, G.; Furthmüller, J. *Comput. Mater. Sci.* 1996, **6**, 15-50.
5. Kresse, G.; Furthmüller, J. *Phys. Rev. B.* 1996, **54**, 11169-11186.
6. Perdew, J. P.; Burke, K.; *Phys. Rev. Lett.* 1996, **77**, 3865-3868.
7. Geng, L.; Cheng, W. D.; Zhang, H.; Lin, C. S.; Zhang, W. L.; Li, Y. Y.; He, Z. Z. *Inorg. Chem.* 2011, **50**, 2378-2384.
8. Bronger W, Bomba C, Fleischhauer J, Rusbüldt, C. *J. Less Common Metals.* 1990, **167**, 161-167.
9. Bronger W, Bomba C. *J. Less Common Metals.* 1990, **158**, 169-176.
10. Han D, Du H, Dai M, Sun D, Chen S. *J. Mater. Chem. A.* 2017, **5**, 6200-6210.